

**Tenfold enhancement of MeV Proton generation by a moderate ultra-short laser  
interaction with H<sub>2</sub>O nano-wire targets**

A. Zigler<sup>1</sup>, T. Palchan<sup>1</sup>, N. Bruner<sup>1</sup>, E. Schleifer<sup>1</sup>, S.Eisenmann<sup>1</sup>,

Z. Henis<sup>1</sup>, M. Botton<sup>1</sup>, S.A. Pikuz<sup>2</sup>, Jr. A.Y. Faenov<sup>2</sup>, D. Gordon<sup>3</sup>, P.Sprangle<sup>3</sup>

(1) Racah Institute of Physics, Hebrew University, Jerusalem 91904, Israel

(2) Joint Institute for High Temperatures, Russian Academy of Sciences, Izhorskaja  
Street 13/19, 127412, Moscow, Russia

(3) Plasma Physics Division, Naval Research Laboratory, Washington, D.C. 20375, USA

*Compact sources of high energy protons (50-500MeV) are expected to be key technology in a wide range of scientific applications [1-8]. Particularly promising is the target normal sheath acceleration (TNSA) scheme [9,10], holding record level of 67MeV protons generated by a peta-Watt laser [11]. In general, laser intensity exceeding  $10^{18}$  W/cm<sup>2</sup> is required to produce MeV level protons. Enhancing the energy of generated protons using compact laser sources is very attractive task nowadays. Recently, nano-scale targets were used to accelerate ions [12,13]. Here we report on the first generation of 5.5-7.5MeV protons by modest laser intensities ( $4.5 \times 10^{17}$  W/cm<sup>2</sup>) interacting with **H<sub>2</sub>O nano-wires** (snow) deposited on a Sapphire substrate. In this setup, the plasma near the tip of the nano-wire is subject to locally enhanced laser intensity with high spatial gradients, and confined charge separation is obtained. Electrostatic fields of extremely high intensities are produced, and protons are accelerated to MeV-level energies. Nano-wire engineered targets will relax the demand of peak energy from laser based sources.*

The protons are obtained from a nano-wires (snow) target that is positioned at the focal point of a 0.5 TW, 40 fsec laser at the Hebrew University High Intensity Laser facility (see Fig. 1a). The laser operates at a central wavelength of 798 nm, and is focused by an off-axis parabolic mirror (F# = 3.3) to a spot size of 80  $\mu\text{m}^2$  (FWHM) on the target. The laser irradiates the snow interface at 60° to the normal. A pre-pulse of time duration of the same time scale as the main pulse, originates in the regenerative pre-amplifier, and precedes the main pulse by 10 nsec. The main pulse to pre-pulse contrast ratio is  $10^3$ . A microscopic imaging system is used to make sure

that the laser irradiates a fresh patch of snow at every shot. The diagnostics of the accelerated protons consist of CR39 SSNTD plates, covered by various layers of B10 and Aluminum foils serving as energy filters. The detector is positioned at a distance of 35 mm from the target's plane along the normal, collecting protons from solid angle of 1.2 sr. A reference CR39 detector is placed at a position hidden from the target to measure the background signal. Each detector with energy filter setup is exposed to a series of 30-50 laser shots before being pulled out of the vacuum chamber and processed.

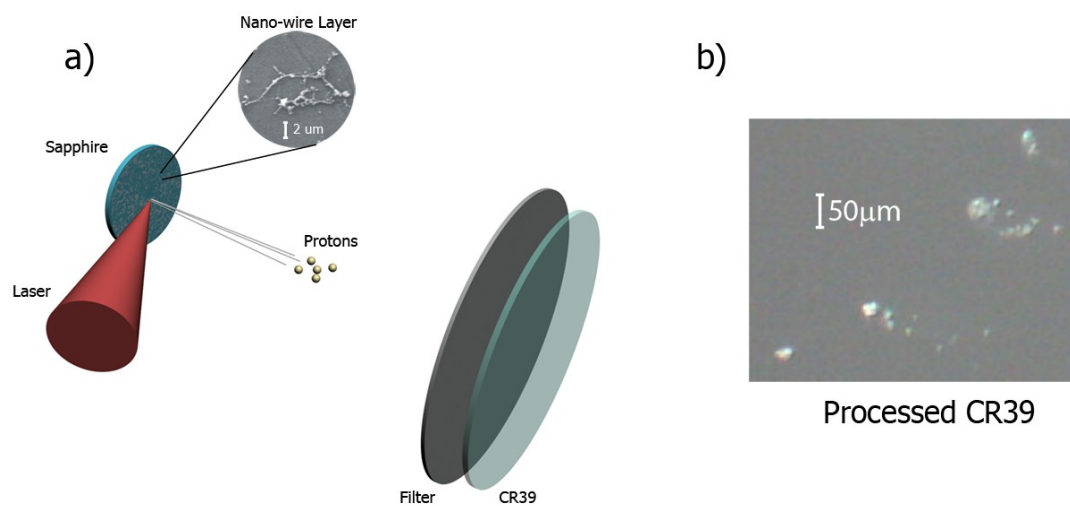


Figure 1: a) Schematics of experimental setup. b) Proton track bunches on a processed CR39 plate.

A typical scan of the processed CR39 detector is shown in Fig. 1b. The proton tracks (bright, circular spots) are accumulated in bunches, with no preferred orientation on the detector plane. Proton bunches are accelerated into relatively small solid angles of about  $1.6 \mu\text{sr}$ . We therefore deduce that a bunch represents several protons accelerated in one shot at the same direction. Considering the stopping power of the

aluminum foil (of thickness 208 $\mu\text{m}$ ) that is placed in front of the CR39 detector, we conclude that the energy of the fastest protons is 5.5-7.5MeV. The number of proton tracks behind the filters is  $4708 \pm 707$  protons/shot/sr compared to a background level of  $2942 \pm 1079$  on the unexposed CR39. Note that the detector is placed at an angle to the laser beam thus the protons are not accelerated along the laser direction as in the planar TNSA experiments. The scaling of the protons energy as a function of the intensity of the main pulse is shown in Fig. 2. The data obtained in the current experiments (HU) follows the conventional relation  $E_{\text{max}} \propto (I\lambda^2)^{0.5}$ , but is achieved with lower energy and intensity levels of the laser.

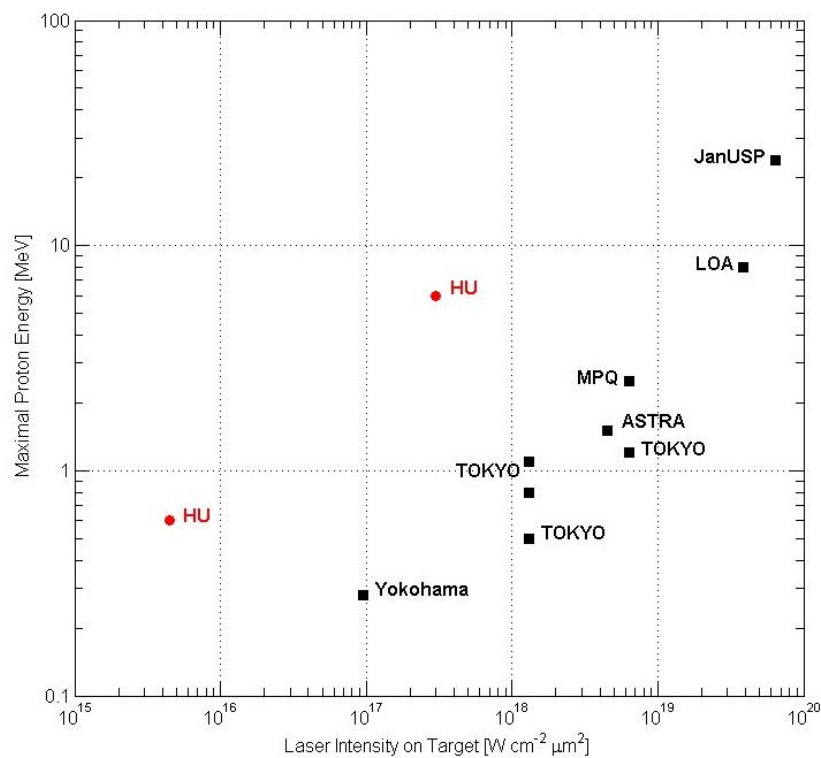


Figure 2: Maximal proton energy in MeV versus the intensity for a short <100 fsec Ti: Sapphire laser systems (Data taken from Ref [3,17])

A possible explanation of the experimental results starts with the assumption that the arrangement of the nano-wires on the target is amorphous due to the deposition method. Based on our previous analysis of the snow target [14,15] we estimate that the distance between adjacent nano-wires ( $\sim 5\text{-}10\mu\text{m}$ ) is large compared to their diameter ( $\sim 0.1\mu\text{m}$ ) (see Fig 1a). Furthermore, the spot size of the laser beam is small enough so that it interacts with few nano-wires. For simplicity, we assume that the laser (pre-pulse and main pulse) interacts with only one nano-wire. The highly efficient absorption of the laser energy by the snow target [14] points to the fact that the pre-pulse completely vaporizes the nano-wire (note that the plasma skin depth is larger than the width of the nano-wire). The temperature of the formed plasma is estimated to be about 2-5eV. During the 10nsec interval between the pre-pulse and the main pulse, the plasma freely expands away from the nano-wire. The main pulse therefore interacts with a non-uniform cylindrical symmetric plasma density (see Fig. 3), unlike the conventional TNSA foil configuration where the laser interacts with constant or planar plasma distribution.

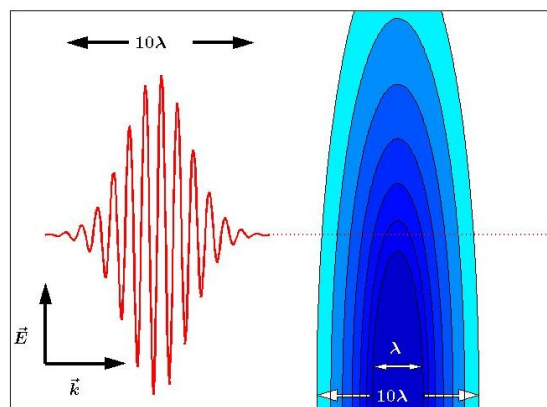


Figure 3: Model - The plasma density (Darker blue represents higher density) in the vicinity of the  $\text{H}_2\text{O}$  nano-wire at the time the main pulse (red on the left) impinges the target.

For brevity of presentation, the main laser pulse is assumed to propagate in a direction perpendicular to the needle symmetry axis. Even with these simplifications the interaction is essentially three dimensional as the laser breaks the cylindrical symmetry of the nano-wire. The main-pulse length is larger than the width of the nano-wire. Accordingly the averaged ponderomotive potential of the laser in the vicinity of the tip can be calculated using the quasi-static approximation. We model the tip as a prolate spheroid with conductivity and dielectric constant related to the plasma parameters. The main result of this model is the field enhancement near the tip by an amount related to the tip radius and the distance from the tip. To obtain a clear, yet representing, one dimensional model of the acceleration process, we analyze the interaction of the laser with the plasma distributed along one ray in parallel to the laser wave-vector. The density profile of the plasma along a ray and the enhancement factor of the laser amplitude due to the tip are described in Fig. 4. We now solve a set of one-dimensional fluid equations for the electrons and ions in a plasma of the given distribution function assuming that the main pulse propagates from the left edge to the right and is subject to the tip enhancement. The effect of the ponderomotive potential in this case is enhanced by two factors. First is the local field enhancement which is translated to direct enhancement of the amplitude. Next is the increment of the gradient of the ponderomotive potential due to the local character of the field enhancement. The plasma electrons are therefore subjected to a greatly increased force and accordingly the density is modified to a greater extent than is expected of the laser intensity by itself. Fig. 4 demonstrates this enhancement. Black line shows the distribution of the electrons after the passage of the laser pulse including the tip enhancement. The exact position and magnitude of

the electron cloud is a function of the maximal enhancement and gradient of the tip. We note that the level to which the electrons are compressed depends also on the temperature they gain in the process. Up to this stage the ions are practically not affected by the laser pulse at all. However, they start to respond to the electrostatic potential of the electrons cloud. Following the conventional model [16], we estimate the temperature of the electrons in the cloud, the scale length that determines the intensity of the accelerating field and the accelerating distance. To estimate the temperature of the electrons we use the following expression:

$$kT_{Hot} \sim m_e c^2 \left[ \sqrt{1 + \frac{a_{tip}^2 I \lambda^2}{1.37 \times 10^{18}}} - 1 \right]$$

Here the conventional scaling of the laser intensity is multiplied by the field enhancement of the tip,  $a_{tip}$  (squared for intensity). Taking this factor to be 10 (which means a modest field enhancement of  $\sim 3$ ) we find that the temperature of the hot electrons in the cloud is of the order of 200-300keV. Next we estimate the scale length of the local plasma using the calculations of the cold fluid model. Based on the fluid model we find that the electrons cloud is ramped up by a steep gradient which is estimated to be 0.1-0.05 $\lambda$  (see Fig. 4). Furthermore, we estimate that the length over which the protons can be accelerated is  $\lambda$ . Combining the above we find that the protons can be accelerated to about 10-20 $kT_{hot}$  which for laser intensity at the range of  $4.5 \times 10^{17}$  W/cm<sup>2</sup> is 2-6MeV. Several remarks are in order. First, we would like to stress that the most energetic protons are accelerated in a direction that is defined by the orientation between the tip and the wave vector of the laser. This is supported by our experimental results where we find bunches of accelerated protons and not a uniform distribution. Furthermore, as this acceleration scheme is

ballistic in nature we do not expect a large amount of protons to reach this energy unless specially designed targets are used. Finally, three-dimensional effects, which will not change the basics of the accelerating scheme, must be considered to describe the exact position of the electron cloud with respect to the tip depending on the parameters of the plasma, the tip and the laser.

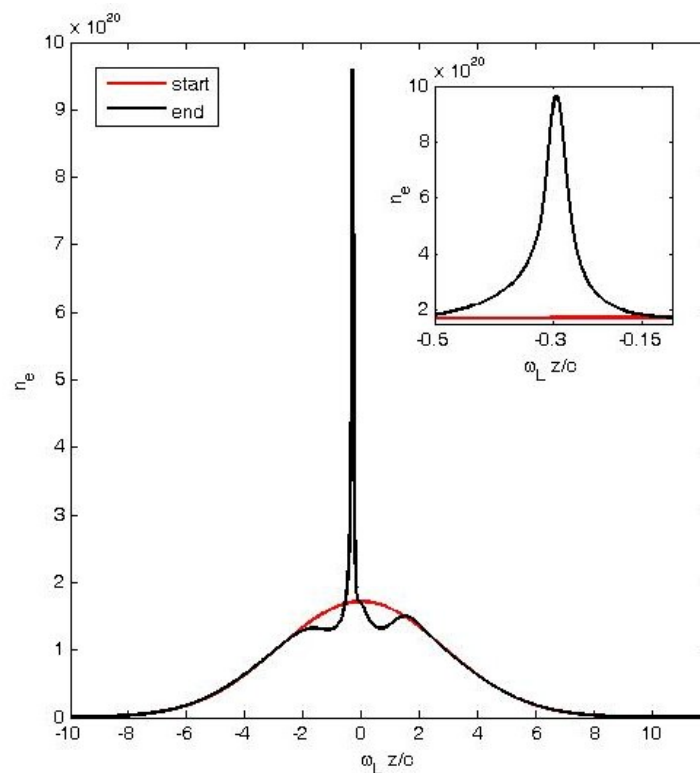


Figure 4: Electron density normalized to the laser frequency before and after the main laser pulse has passed the H<sub>2</sub>O nano-wire. Inset: Zoom on the region of peak electron density.

In conclusion, we have experimentally demonstrated generation of 5.5-7.5 MeV protons from snow nano-wire targets by modest,  $4.5 \times 10^{17}$  W/cm<sup>2</sup> laser intensities, which is an order of magnitude higher compared with previous experiments with such laser intensities. The protons are accelerated by the enhanced interaction of the laser field and the plasma near the tip of the nano-wire. Engineered nano-wire



targets can improve the interaction scheme by increasing the number of accelerated protons and directing them in a pre-designed direction.

## METHODS

**Laser.** The experiments were performed using the HU-HIL facility, a TW-level Ti:Sapphire chirped pulse amplification system. It is capable of delivering laser pulses of up to 20mJ with  $40 \pm 5$  fsec FWHM pulse duration. Using an off-axis parabolic mirror ( $F\# = 3.3$ ) to a spot size of  $80 \mu\text{m}^2$  (FWHM) reaching an intensity of  $4.5 \times 10^{17}$  W/cm<sup>2</sup> on the target. The temporal duration is monitored using SHG autocorrelator system. A pre-pulse originating in the regenerative pre-amplifier which arrives to the target 10 nsec before the main pulse is  $10^3$ . Pulse length and focal spot size are measured at the beginning of every series of shots. The intensity of the main laser pulse and pre-pulse contrast ratio are measured once every several shots. The laser operated at a central wavelength of 798nm with a repetition rate of 10 Hz. Selection of a single pulse is possible using a fast mechanical shutter.

**H<sub>2</sub>O nano-wire target.** A 600 $\mu\text{m}$  thick Sapphire substrate is thermally coupled to a copper box and placed inside a vacuum chamber. At the beginning of the process the air from the vacuum chamber is pumped out. The substrate is then cooled by a constant flow of liquid nitrogen. After the temperature drops down to 110°K H<sub>2</sub>O vapor is supplied using a needle valve which inserts the vapor close to cooled substrate. It takes about 10 minutes for the vapor to condensate on the plate and to form nano-wire layers of snow with 100 $\mu\text{m}$  thickness. After the snow is fully grown the chamber is pumped again to reach the suitable vacuum ( $<10^{-4}$  mbar) for the experiments.

**Proton detection.** Protons accelerated from the nano-wire were detected on a nuclear track detector CR39 (produced by Intercast Europe). In front of the CR39 plates we placed up to 4 layers of B10 film serving as a ~0.5 MeV filter and 208 $\mu$ m of Aluminum foils which serve as 5.5MeV filter. The energy of the protons that pass a particular foil thickness was calculated using TRIM and SRIM (by J.F. Ziegler for the calculation of transport, stopping power and range of ions in matter - <http://www.srim.org>). After exposure, the plates were etched in a 3N KOH solution at 80°C, which corresponds to 2 $\mu$ m/h bulk etch rate. After the etching, the protons tracks became visible and could be investigated using a X40 microscope.

## References

1. Hegelich, B. M. et al. Laser acceleration of quasi-monoenergetic MeV ion beams. *Nature* **439**, 26 (2006).
2. Schwoerer, H. et al. Laser–plasma acceleration of quasi-monoenergetic protons from microstructured targets. *Nature* **439**, 445 (2006).
3. Fuchs, J, et al. Laser acceleration of low emittance, high energy ions and applications. *C. R. Physique* **10**, 176 (2009).
4. Nickles, P. V. et al. Ultrafast laser-driven proton sources and dynamic proton imaging. *J. Opt. Soc. Am. B* **25**, B155 (2008)
5. Sarri, G. et al. The application of laser-driven proton beams to the radiography of intense laser–hohlraum interactions. *New J. Phys.* **12**, 045006 (2010).
6. Fritzier, S. et al. Proton beams generated with high-intensity lasers: Applications to medical isotope production. *App. Phys. Lett.* **83**, 3039 (2003).
7. Roth, M. et al. Fast ignition by intense laser-accelerated proton beams. *Phys. Rev. Lett.* **86**, 436 (2001).
8. Ledingham, K. Going up? K. *Nature* **2**, 11 (2006).
9. Hatchett, S. et al. Electron, photon, and ion beams from the relativistic interaction of Petawatt laser pulses with solid targets. *Phys. Plasmas* **7**, 2076 (2000).
10. Wilks, S. et al. Energetic proton generation in ultra-intense laser–solid interactions. *Phys. Plasmas* **8**, 542 (2001).

11. Gaillard, S. A. et al. 65+ MeV protons from short-pulse-laser micro-cone-target interactions. In Proc. APS 51<sup>st</sup> Annual meeting of the APS Division of Plasma Physics, Abstract G06.003 (2009).
12. Bagchi, S. et al. Fast ion beams from intense, femtosecond laser irradiated nanostructured surfaces. *Appl. Phys. B* **88**, 167–173 (2007)
13. Ramakrishna, B. et al. Laser-driven quasimonoenergetic proton burst from water spray target. *Phys. Plasmas* **17**, 083113 (2010)
14. Palchan, T. et. al. Efficient coupling of high intensity short laser pulses into snow clusters. *App. Phys. Lett.* **90**, 041501 (2007).
15. Palchan, T. et. al. Generation of fast ions by an efficient coupling of high power laser into snow nanotubes. *App. Phys. Lett.* **91**, 251501 (2007).
16. Wilks, S. C. and Kruer, W.L. *IEEE J Quantum Elect.* **33**, 1954 (1997).
17. Borghesi, M. et al. Fast ion generation by high-intensity laser irradiation of solid target and applications. *Fusion Sci. Technol.* **49**, 412 (2006).